Intuitive Modeling of Folds and Wrinkles in a Cloth Simulation

Wu Shin-Ting Leandro Pinho de Monteiro
State University of Campinas
School of Electrical and Computer Engineering
Campinas, São Paulo, Brazil
{ting,lpm}@dca.fee.unicamp.br

Abstract

Cloth modeling and animation aiming high realistic visual effects are very complex processes. It may involve the formulation of a physically-based model, collision detection and response techniques, and a time-consuming integration numerical solver. This is because cloth presents a very peculiar behavior. It bends easily, while hardly stretches. Folds naturally appear and disappear, yielding diverse wrinkles and buckles, which are recognized to be fundamental for realistic simulations. Modeling these phenomena, and yet, controlling the aspect of folds without resorting to artificial forces is a field that still needs improvements. In this paper we analyze the interdependence of the parameters in the deformable surface model proposed by Melo and propose a geometry oriented control that is suitable for generating a large variety of folds and wrinkles.

1. Introduction

Cloth modeling is of particular interest in several applications, ranging from the entertainment and advertisement purposes to the highly lucrative fashion business. Although a variety of strategies for the computer support of cloth modeling and animation has been rapidly evolved since the mid seventies, realistic garment deformations while a character's body moves is still a challenging problem. This is because that fabrics are smooth surfaces possessing a complex structure consisting of interwoven threads, which are themselves made of twisted fibers. The frictional (internal) forces between these fibers give the fabric a very peculiar physical behavior. It strongly resists to the length/area variations while is being very permissive to form wrinkles and folds.

Some works have been devoted to modeling the cloth bending behaviors [2, 3, 4, 8, 15]. They are based on the approach that keeps apart the in-plane and the out-plane deformations, such that the total internal energy is expressed as the sum of the energies accumulated due to these two deformations. The pitfall of this approach is that the compatibility relation between these two deformations are overlooked, thus may lead to a configuration that does not resemble cloth if fictitious damping forces are not added. Appropriate setting of these forces is not an easy task. On the basis of the theory of a Cosserat surface [7], Melo proposed a bending model which takes into account this compatibility condition. One of the features of the proposed bending model is that its parameters have clear geometric interpretations, making control easier. Instead of the in-plane and bending energies, his model contains one more term: the coupling term of the in-plane and bending deformations [9]. Pinho and Wu presents an implementation of this model with use of an explicit integration method [10]. Realistic simulations have been achieved. This paper further discusses one of the remaining problem: how to manipulate the parameters of this bending model to get pleasing simulation results.

In this paper, we present the results of our investigation on the calibration of those parameters in order to obtain a variety of folds and buckling in distinct textile materials under different force conditions, such as the ones presented in Figure 1. We developed an interactive interface that facilitates our experiments. The parameters that we used are furnished to show the correspondence between the provided numerical values and the pleasing visual effects. The main conclusion of our study is that the model may deliver convincing visual bending effects by adjusting a relatively few and geometrically interpretable parameters, namely the resistance to in-plane variations, the resistance to out-plane deformations, and the easiness to buckling formation.

The rest of the paper is organized as follows. Section 2 describes briefly the bending model proposed by Melo, focusing mainly on the set of parameters necessary for modeling the cloth's dynamics, and Section 3 shows the interface we designed to this bending model for investigating the dependence of its parameters. In Section 4 we present a procedure that we adopted for getting the parameter values to

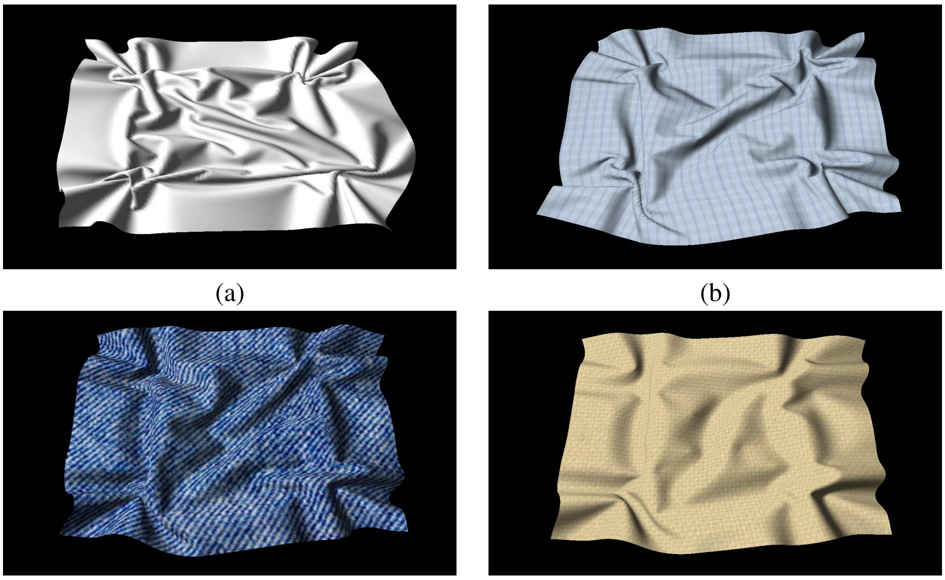

(a)

(b)

(c)

(d)

Figure 1. Buckling effects on distinct textile materials: (a) satin, (b) cotton, (c) jeans, (d) sailcloth.

simulate the behavior of different cloth materials. Section 5 provides a variety of folds and buckling we have achieved with this procedure. Concluding remarks and further work are given in Section 6.

2. Cloth Model

To be self-contained, the deformable surface model proposed by Melo is summarized. The main contribution of his work is to devise a novel formulation for the internal forces $\frac{\delta \mathcal{A}(\mathbf{r},t)}{\delta \mathbf{r}}$ that appear in the well-known ordinary differential equation that governs a surface's dynamics [14]

$$\mu \frac{\partial^2 \mathbf{r}}{\partial t^2} + \varrho \frac{\partial \mathbf{r}}{\partial t} + \frac{\delta \mathcal{A}(\mathbf{r}, t)}{\delta \mathbf{r}} = \mu \mathbf{F}(\mathbf{r}, t) \ , \tag{1}$$

where μ is the mass density (mass per unit area), ϱ is the coefficient of the damping forces and $\mathbf{F}$ denotes the total contribution of external forces per unit mass on each surface point $\mathbf{r}$.

Melo models his deformable surface as a particular case of the general theory of a Cosserat surface. The theory of a Cosserat surface is exact, complete, and fully consistent with dynamical and thermodynamical principles of continuum mechanics. It was originally proposed by the Cosserats in 1909, rediscovered during the 50s for oriented bodies modeling [5] and, later, for shell modeling [7]. A Cosserat surface is a surface embedded in R^3 to whose every point an out-of-plane vector $\mathbf{d}$, called a *director*, is assigned.

Applying the general Cosserat's shell theory to cloth modeling is not a novelty. Eischen et al. present in [6] a cloth model founded on a Cosserat surface, after the publication of a series of three papers by Simo et al, in which they demonstrate that, despite its awkward formulation, a classical shell theory is conducive to an efficient numerical implementation [11, 12, 13]. The key point for their finding is a new parametrization that avoids the terms such as the Christoffel symbols and the coefficients of the second fundamental form. The price that they pay is to adopt relations that do not explicitly associate shape quantities with the textile mechanics ones. Melo [9] demonstrates that modeling the cloth as an inextensible normal-director elastic Cosserat surface, that is by assuming that the director vector corresponds to unitary normal vector, we may get an algebraic expression for the internal energy that is familiar to the graphics community, with explicit relations between the geometrical and statical quantities.

Throughout this section, Latin indexes will have the range $1, 2, 3$ whereas Greek indexes with the range $1, 2$ are used for components of space tensor or components of surface tensor. We also adopt the summation convention which consists in omitting the sign $\sum$. If in a product a Greek letter figures twice, once as superscript and once as subscript, summation must be performed from 1 to 2 with respect to this letter, and if a Latin letter appears, summation must be carried out from 1 to 3 [1].

We may represent a cloth $\mathcal{S}(t) = \mathbf{r}(x^1, x^2, t)$ as an elastically deformable surface at time t. Let x^1- and x^2-curves be the coordinate curves lie on $\mathcal{S}$ and x^3 be along the normal to $\mathcal{S}(t)$. The x^i are identified as *convected coordinates* because any point on $\mathcal{S}$ has the same curvilinear coordinates in the reference state and in the deformed state. The first derivatives along the x^α-curves

$$\mathbf{a}_\alpha(t) = \frac{\partial \mathbf{r}}{\partial x^\alpha}(t) \tag{2}$$

and the unit normal to $\mathcal{S}(t)$

$$\mathbf{n}(t) = \mathbf{a}_3(t) = \frac{\frac{\partial \mathbf{r}}{\partial x^1}(t) \times \frac{\partial \mathbf{r}}{\partial x^2}(t)}{|\frac{\partial \mathbf{r}}{\partial x^1}(t) \times \frac{\partial \mathbf{r}}{\partial x^2}(t)|} \tag{3}$$

are linearly independent and build the *base vectors* of a *moving trihedron*, of which $\frac{\partial \mathbf{r}}{\partial x^1}$ and $\frac{\partial \mathbf{r}}{\partial x^2}$ lie in the tangent plane normal to $\mathbf{n}$. It is assumed that the director vector $\mathbf{d}(t)$ of $\mathcal{S}(t)$ always follows the variation of the normal vector at any time t. Hence, it does not suffer any displacements with respect to the moving trihedron.

The metric and curvature tensors of $\mathcal{S}(t)$ are, respectively, given by

$$a_{\alpha\beta}(t) = a_{\alpha\beta}(\mathbf{r}(x^1, x^2, t)) = \frac{\partial \mathbf{r}}{\partial x^\alpha}(t)\frac{\partial \mathbf{r}}{\partial x^\beta}(t) \tag{4}$$

and

$$b_{\alpha\beta}(t) = b_{\alpha\beta}(\mathbf{r}(x^1, x^2, t)) = \mathbf{n}(t) \cdot \frac{\partial^2 \mathbf{r}(t)}{\partial x^\alpha \partial x^\beta}. \tag{5}$$

Moreover, the coefficients $a^{\alpha\beta}$ of the inverse matrix of the matrix formed by $a_{\alpha\beta}$ are

$$a^{11} = \frac{a_{22}}{a},\ a^{12} = a^{21} = -\frac{a_{12}}{a},\ a^{22} = \frac{a_{11}}{a}. \tag{6}$$

Particularly, at $t = t_0$ we refer the undeformed surface by $\mathcal{S}(t_0) = \mathbf{R}(x^1, x^2) = \mathbf{r}(x^1, x^2, t_0)$ and its metric and curvature tensors by $A_{\alpha\beta} = a_{\alpha\beta}(t_0)$ and $B_{\alpha\beta} = b_{\alpha\beta}(t_0)$.

With use of the elements of metric and curvature tensors, two kinematics variables of $\mathcal{S}$ are defined:

1. **Membrane strains** ($\varepsilon_{\alpha\beta}$)

$$\varepsilon_{\alpha\beta} = \frac{1}{2}(a_{\alpha\beta} - A_{\alpha\beta}) \tag{7}$$

2. **Bending strains** ($\kappa_{\beta i}$)

$$\kappa_{\beta\alpha} = -(b_{\beta\alpha} - B_{\beta\alpha}). \tag{8}$$

An approximation to the internal energy $\mathcal{A}$ of $\mathcal{S}$ may be given in terms of these quantities and the parameters that characterize the surface material properties, $\Phi^{\alpha\beta}$, $\Psi^{\alpha\beta}$ and $\Theta^{\alpha\beta}$

$$\mu_0 \mathcal{A} = \left[\Phi^{\alpha\beta}\varepsilon_{\alpha\beta}\varepsilon_{\lambda\rho} + \Psi^{\alpha\beta}\kappa_{\alpha\beta}\kappa_{\lambda\rho} + \Theta^{\alpha\beta}\varepsilon_{\alpha\beta}\kappa_{\lambda\rho}\right] \tag{9}$$

The first and second terms on the right-hand side of Eq. 9 are the quadratic forms of the stretching and bending measures, respectively, while the third term, containing products of stretching and bending measures, represents a coupling of stretching and bending effects.

The surface material properties are, in their turn, expressed in terms of the coefficients $A^{\alpha\beta}$ of the inverse matrix of the matrix built by the metric tensors $A_{\alpha\beta}$ in the reference state:

$$\begin{aligned}
\Phi^{\alpha\beta} &= \Phi^{\beta\alpha} = \zeta_{\alpha\beta}(A^{\alpha\alpha}A^{\beta\beta} + 2(A^{\alpha\beta})^2) \\
\Psi^{\alpha\beta} &= \Psi^{\beta\alpha} = \xi_{\alpha\beta}(A^{\alpha\alpha}A^{\beta\beta} + 2(A^{\alpha\beta})^2) \\
\Theta^{\alpha\beta} &= \Theta^{\beta\alpha} = \phi_{\alpha\beta}(A^{\alpha\alpha}A^{\beta\beta} + 2(A^{\alpha\beta})^2),
\end{aligned} \tag{10}$$

where $\zeta_{\alpha\beta}$ and $\xi_{\alpha\beta}$ are *elasticity coefficients* and $\phi_{\alpha\beta}$ is called the *buckling factor*.

The derivatives of the internal energy $\mathcal{A}$ are

$$\begin{aligned}
\mu\frac{\partial \mathcal{A}}{\partial \varepsilon_{\alpha\beta}} &= N^{*\alpha\beta} = \frac{\mu}{\mu_0}(2\Phi^{\alpha\beta}\varepsilon_{\alpha\beta} + \Theta^{\alpha\beta}\kappa_{\alpha\beta}) \\
&= \frac{\mathcal{S}_0}{\mathcal{S}}(2\Phi^{\alpha\beta}\varepsilon_{\alpha\beta} + \Theta^{\alpha\beta}\kappa_{\alpha\beta}) \\
\mu\frac{\partial \mathcal{A}}{\partial \kappa_{i\alpha}} &= M^{\alpha\beta} = \frac{\mu}{\mu_0}(2\Psi^{\alpha\beta}\varepsilon_{\alpha\beta} + \Theta^{\alpha\beta}\kappa_{\alpha\beta}) \\
&= \frac{\mathcal{S}_0}{\mathcal{S}}(2\Psi^{\alpha\beta}\varepsilon_{\alpha\beta} + \Theta^{\alpha\beta}\kappa_{\alpha\beta}),
\end{aligned} \tag{11}$$

where μ and μ_0 are, respectively, the mass density at time t and t_0 per unit area of $\mathcal{S}$.

Once the following equality is valid for the components $N^{\alpha\beta}$

$$N^{\alpha\beta} = N^{*\alpha\beta} - b^\alpha_\lambda M^{\beta\lambda}, \tag{12}$$

with $b^\alpha_\lambda = a^{\rho\alpha}b_{\lambda\rho}$ relating the membrane and the bending deformations, if we neglect the forces acting on the director vectors, we may express the internal forces as the covariant derivative of the in-plane forces $\mathbf{N}^\alpha$

$$\begin{aligned}
\mathbf{N}^\alpha{}_{|\alpha} &= \frac{\delta \mathcal{A}(\mathbf{r}, t)}{\delta \mathbf{r}} = \left[(N^{\beta\alpha}\mathbf{a}_\beta)_{,\alpha} + \Gamma^\lambda_{\alpha\lambda}N^{\beta\alpha}\mathbf{a}_\beta\right] \\
&+ \left[(M^{\alpha\beta}{}_{|\beta}\mathbf{a}_3)_{,\alpha} + \Gamma^\lambda_{\alpha\lambda}M^{\alpha\beta}{}_{|\beta}\mathbf{a}_3\right].
\end{aligned} \tag{13}$$

Summarizing, Eq. 1 tells us that the dynamics of a deformable surface is governed by its mass μ, the derivatives of its internal energy, and the external forces. The internal energy formulation consists of the sum of component energies weighted by the constants $\zeta_{\alpha\beta}$, $\xi_{\alpha\beta}$ and $\phi_{\alpha\beta}$. Attributing high values to $\zeta_{\alpha\beta}$, Pinho and Wu successfully apply this model in cloth simulations [10].

3. Graphics Interface

In this section we present the graphics interface we designed to the cloth model described in Section 2. We aim at perceiving the role that each parameter of this model plays along the simulation and empirically assigning to it a dominant independent rule in such a way that all possible values combinations could generate the set of all desirable visual effects

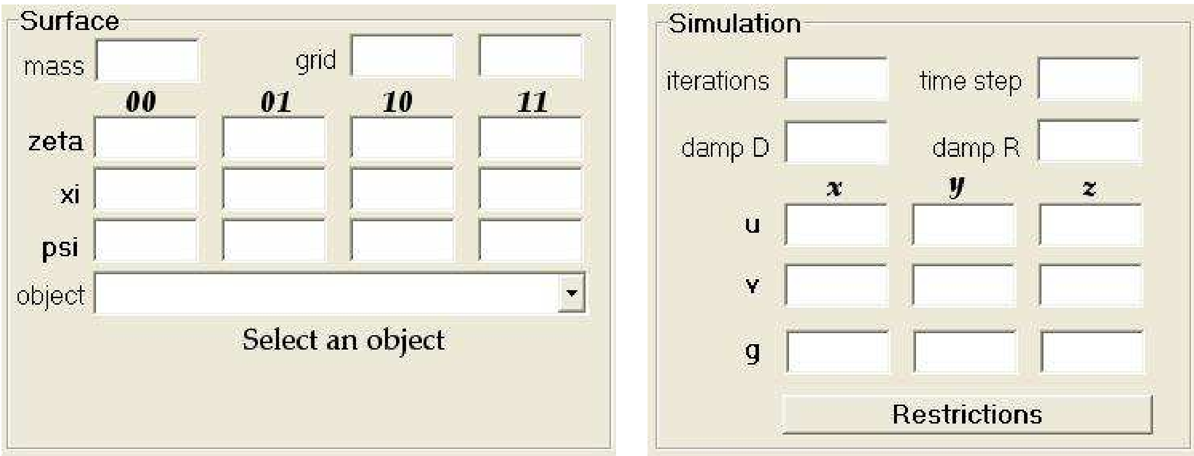

(a) (b)

Figure 2. User interface.

It is worth remarking that to improve the realism in the motion of a deforming surface $\mathcal{S} = \mathbf{r}(x^1, x^2, t)$ under the force $\mathbf{F}$ per unit mass, we should consider its inertial forces as well as the viscous forces generated by the deforming surface as it interacts with the fluid of density ϱ that fills the ambient space. In the implementation presented by Pinho and Wu, they consider that there are friction forces acting in a direction parallel to the surface's trajectory and these forces are linearly proportional to velocity

$$\mathbf{F}_D = \varrho_D \frac{\partial \mathbf{r}}{\partial t}. \tag{14}$$

and for simulating the fluid drag, such as the wind drag, they simply adopt the following equation [14]

$$\mathbf{F}_R = \varrho_R(\mathbf{n} \cdot (\mathbf{u} - \mathbf{v}(t))\mathbf{n},$$

where $\mathbf{u}$ is the fluid's velocity. Hence, the kinematics of the deforming surface is described by

$$\mu \frac{\partial^2 \mathbf{r}}{\partial t^2} + \varrho_D \frac{\partial \mathbf{r}}{\partial t} - \varrho_R(\mathbf{n} \cdot (\mathbf{u} - \mathbf{v}(t)))\mathbf{n} = \mu \mathbf{F}(t) = \mathbf{f}(t). \tag{15}$$

For sufficiently small variations, in which the linearity is observed, we may apply the superposition principle and sum the effects due to Eq. 14 and Eq. 15 to find the total resultant on the position vector $\mathbf{r}$ at time t

$$\mu \frac{\partial^2 \mathbf{r}}{\partial t^2} - \mathbf{N}^{\alpha}_{|\alpha}(t) = \mathbf{f}(t) - \varrho_D \mathbf{v}(t) + \varrho_R(\mathbf{n} \cdot (\mathbf{u} - \mathbf{v}(t)))\mathbf{n}. \tag{16}$$

According to the physical interpretation, we make a distinction of three classes of parameters, which are organized in two panels containing line edit, label, button, and combo box widgets (Figure 2):

1. Kinematics parameters are the parameters that characterize the initial state of the deformable surface or that depend on the ambient space. They are the damping coefficients due to the friction forces of the ambient space (ϱ_R and ϱ_D), the fluid velocity ($\mathbf{u}$), and the initial velocity of $\mathcal{S}$ ($\mathcal{V}_0$).
2. Simulation parameters are the parameters necessary for simulations and numerical solutions. They are the spatial discretization (Δ), the time Step (Δt), the external forces (f), and the number of Iterations. In the current implementation, for external forces of form $\mu\mathbf{g}$, only the value of $\mathbf{g}$ should be provided. Additional external forces must be defined as further Restrictions.
3. Material parameters are the parameters that define the intrinsic characteristic of the textile. They are mass density (μ), metric elasticity coefficients ($\zeta_{\alpha\beta}$), bending elasticity coefficients ($\xi_{\alpha\beta}$), and buckling factor ($\phi_{\alpha\beta}$).

In Figure 2.a the elasticity coefficients $\zeta_{\alpha\beta}$, $\xi_{\alpha\beta}$, and $\phi_{\alpha\beta}$ correspond to zeta, xi, and psi, respectively. mass denotes the total mass of the simulated object object and through grid we specify the spatial discretization. Figure 2.b presents the panel containing line edit widgets for specifying the two damping coefficients (damp R and damp D) the fluid's velocity (u), the initial velocity (v), and the acceleration value (g).

The focus of this work is to analyze the effects of the material parameters in the simulation of textile behavior, more specifically in the buckling formation. We observe that the elasticity coefficients and the buckling factor are, indeed, lists of 4 values. This is because that the model considers that the deformable surface may have distinguishing behaviors in four directions. When $\alpha \neq \beta$ they act in the diagonal directions with respect to the base vectors, otherwise their effects are the off-diagonal ones. The off-diagonal elasticity coefficients may be different in the directions x^1 and x^2, which allows us to distinguish isotropic from anisotropic textile materials. In our experiments, we only considered isotropic cases, thus the 4 values are identical.

4. Parameter Calibration

Observing Eqs. 11 and 16 we will see that the geometric shape of a deformable surface can be controlled not only by the surface mass, the ambient viscosity, and the external forces, but also by the elasticity parameters and the buckling factor. Due to the diversity of parameters involved, different combinations of those parameters could take us to the same visual effect. For example, to generate the animation of an oscillating surface, we can apply sinusoidal forces to each point of the surface, or we can assign distinct values of ϱ_R and ϱ_D to each point, or assign different values to μ in each point, or we can even define convenient values for the elasticity parameters. This flexibility increases the model's versatility, but, on the other hand, makes it difficult to be controlled, since these parameters are not orthogonal and the influence of some parameter value can be masked by another's. In this section we deal with this issue more profoundly.

4.1. Analysis

As far as possible, we choose the parameter values that are physically valid, such as the external forces and the mass density. From our exhaustive experiments, we observe that $\zeta_{\alpha\beta}$, $\xi_{\alpha\beta}$ and $\phi_{\alpha\beta}$ possess clear geometrical interpretations. The term weighted by $\zeta_{\alpha\beta}$ is directly related with the in-plane deformations, the one weighted by $\xi_{\alpha\beta}$ has predominant influence on the bending behaviors, and the last term prevalently controls the way that the surface moves out-of-plane under in-plane forces.

For illustration, we simulate the distension of a piece of lycra. Figure 3.a shows the simulation result with $\zeta_{\alpha\beta} = 100$, $\xi_{\alpha\beta} = 0.05$, and $\phi_{\alpha\beta} = 0$. If we set $\zeta_{\alpha\beta} = \xi_{\alpha\beta} = \phi_{\alpha\beta} = 0$, the geometry tends to stretch rapidly and becomes a physically unrealizable surface (Figure 3.b). Maintaining $\zeta_{\alpha\beta}$ and $\phi_{\alpha\beta}$, but attributing $\xi_{\alpha\beta} = 0$, the piece offers no resistance to bending and may present developable undulations, such that the compatibility conditions are satisfied. The result is presented in Figure 3.c. Finally, if we impose resistance to stretch and bending and only consider $\phi_{\alpha\beta} = 0$, the piece appears firmer and no buckling is noticeable (Figure 3.d).

Theoretically, $\zeta_{\alpha\beta}$ weight the variations of the surface's area. It is expected that the higher are their values, the more resistant are the materials to such variations. Figure 4 presents the simulations of a melting cheese ($\zeta_{\alpha\beta}$ have lower values) and a very rigid metallic plate ($\zeta_{\alpha\beta}$ assume higher values), under gravity forces. As most cloth is resistant to metric variations, we should choose large values to the parameters $\zeta_{\alpha\beta}$ in our simulations.

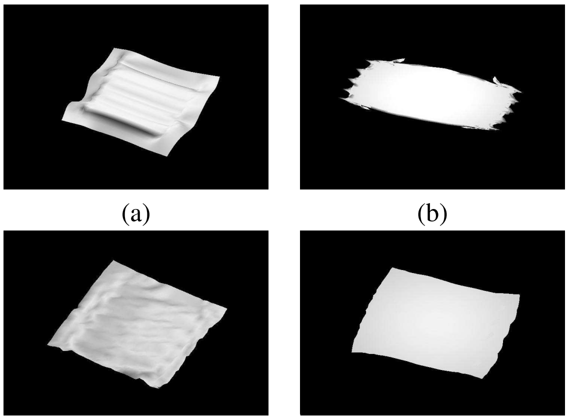

(a) (b) (c) (d)

Figure 3. Influence of elasticity constants and buckling factor in the deformation.

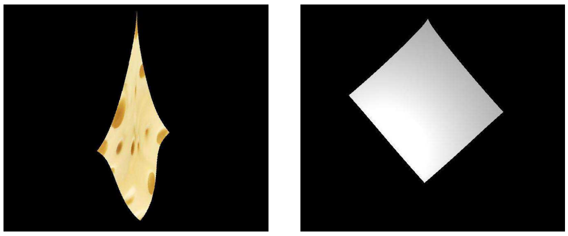

low $\zeta_{\alpha\beta}$ high $\zeta_{\alpha\beta}$

Figure 4. Effects of $\zeta_{\alpha\beta}$ on metric variations.

The parameters $\xi_{\alpha\beta}$ weight the variations of the components of the curvature tensors. The higher are their values, the more resistant is the surface to curving. However, we observed that in a surface with lower resistance to stretching the differences are almost unperceptive when we vary the values from $\xi_{\alpha\beta} = 0.001$ (Figure 5.a) to $\xi_{\alpha\beta} = 0.1$ (Figure 5.b). An explanation for this behavior is that the metric deformations are dominant over the bending variations.

In the case of cloth, which has high resistance to metric variations, the effects of the parameters $\xi_{\alpha\beta}$ are noticeable. In most of cases, it predominantly affects the hardness of curving. We observed that the higher the values of $\xi_{\alpha\beta}$ are, the harder are the folds that are formed. Figure 6 compares the draping of a tablecloth with the possessing greater values of $\xi_{\alpha\beta}$. The first one resembles satin while the second looks like to be made from linen.

The effects of the parameters $\phi_{\alpha\beta}$ are subtle. We may only distinguish them when we apply forces that are par-

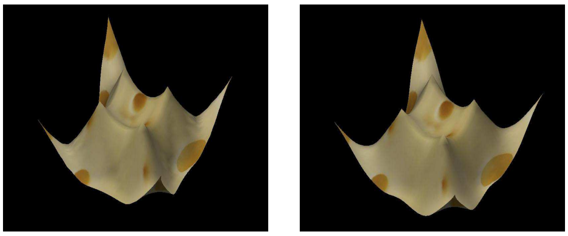

(a) (b)

Figure 5. Effects of $\xi_{\alpha\beta}$ in conjunction with $\zeta_{\alpha\beta}$.

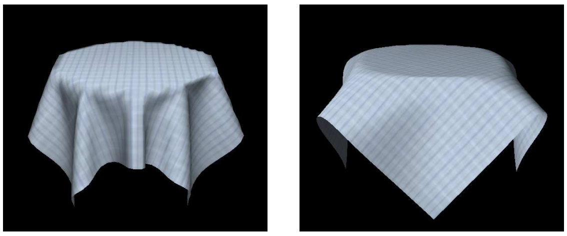

(b) low $\xi_{\alpha\beta}$ (c) high $\xi_{\alpha\beta}$

Figure 6. Effects of $\xi_{\alpha\beta}$.

allel to the surface. Usually, forces parallel to a surface yield either distensions or contractions. But, if the surface has higher resistance to metric variations, such as a cloth, these metric variations should not occur and, because of the compatibility condition. The applied energy is, then, transformed into the bending energy. There are still two ways to bend a surface, which may be controlled by $\phi_{\alpha\beta}$: in-plane and out-of-plane, that is upward with respect to the surface. Figure 7 illustrates visually their contributions to the shape of a deforming surface. Despite lower resistance to curving, observe that, with $\phi_{\alpha\beta} = 0$, the surface tends to preserve its local planarity (Figure 7.a). When we superposed the coupling term, buckling has been naturally formed (Figure 7.b).

For numerical comparison purpose, we summarize in Table 1 the values of parameters $\zeta_{\alpha\beta}$, $\xi_{\alpha\beta}$, $\phi_{\alpha\beta}$ that we used in all simulations presented previously. We remark that the relation of these data is compatible with the relation of the visual effects we achieved: the greater are the values, the firmer seem the material.

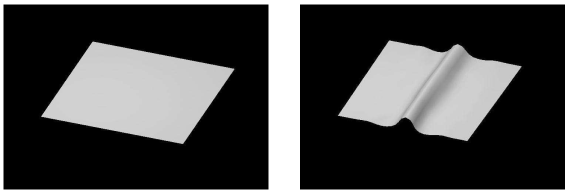

(a) (b)

Figure 7. The appearance of the deforming surface under axial forces (a) without and (b) with coupling term.

Images	μ (g/m^2)	$\zeta_{\alpha\beta}$	$\xi_{\alpha\beta}$	$\phi_{\alpha\beta}$
Figure 1(a)	78	400	0.01	0.1
Figure 1(b)	88	400	0.02	0.1
Figure 1(c)	111	400	0.04	0.1
Figure 1(d)	133	400	0.1	0.1
Figure 3(a)	80	30	0.01	0.1
Figure 3(b)	80	0	0	0
Figure 3(c)	80	30	0	0.1
Figure 3(d)	80	30	0.01	0
Figure 4(a)	200	30	0.05	0
Figure 4(b)	400	1000	10.0	0
Figure 5(a)	200	30	0.01	0.1
Figure 5(b)	200	30	0.05	0.1
Figure 6(a)	100	400	0.01	0.1
Figure 6(b)	100	400	0.05	0.1
Figure 7(a)	78	400	0.01	0
Figure 7(b)	78	400	0.01	0.1
Figure 8(a)	400	100	0.01	0.1
Figure 8(b)	400	120	0.04	0.1
Figure 9(a)	100	400	0.04	0.01
Figure 9(b)	100	400	0.02	0.01
Figure 9(c)	100	400	0.04	1.0
Figure 9(d)	100	400	0.02	1.0

Table 1. Parameters of simulations.

4.2. Procedure

We propose the following procedure consisting of five passes to obtain reasonable material parameters for simulating distinct fabrics:

1. A set of forces is defined in analogy to real physical situations.
2. The mass density of the textile is estimated on the basis of the technical specifications provided by its suppliers.
3. Considering $\xi_{\alpha\beta} = \phi_{\alpha\beta} = 0$, we vary the values of $\zeta_{\alpha\beta}$ until no stretching is visually perceived. We get an interval of values, from which we choose $\zeta_{\alpha\beta} = 400$, which is valid for the textiles we worked with. Nevertheless, we observed that $\zeta_{\alpha\beta}$ is dependent on the

weight of the cloth. The heavier it is, the higher should be the value.

4. Fixing $\zeta_{\alpha\beta} = 400$ and maintaining $\phi_{\alpha\beta} = 0$, we tested empirically several values of $\xi_{\alpha\beta}$ for two samples of textile, until the simulation results are visually comparable with real situations: silk (very soft material) and sailcloth (very stiff material). From these two extremes, we estimated the values of $\xi_{\alpha\beta}$ for other materials on the basis of intuitive evaluation of its degree of hardness with respect to silk. Observe in Table 1 that we have attributed the same value to the coefficients $\zeta_{\alpha\beta}$ of a and varied their parameters $\xi_{\alpha\beta}$, in order to get different curving effects. We adopted the similar strategy for controlling the curving behavior of heavier textile materials.
5. Established the values of $\zeta_{\alpha\beta}$ and $\xi_{\alpha\beta}$, we determine the values of $\phi_{\alpha\beta}$ by applying pure compression and distension forces on each type of textile and comparing the visual effects with the real ones. The greater are the values, the higher is the height of the buckles.

5. Simulation Examples

In this section, we present some garment simulation examples and comment a few aspects related to the combinations of parameter values for obtaining pleasing visual effects of a large range of textile materials.

All the simulations were run on an AMD Athlon 64 3200+ with 512MB of memory, equipped with a NVIDIA GeForce FX 5900 with 128 MB. In all simulations, the following parameters are used: damping coefficient = 0.2 $\frac{kg}{m^2 s}$, Δt = 0.001s, number of renderable frames = 400, total simulation time=20s. The size of the grid is 60×60 (3600 vertices) with $\Delta = 0.01$ unit. The weight of the materials has been obtained from the fabrics suppliers. In all of our simulations we get good results considering that cloth is an isotropic material with high resistance to stretching ($\zeta_{\alpha\beta} = 400$).

Our first example involves the formation of buckling in a bow tie. The physical parameters μ, γ and $\vec{f}$ and the tie dimensions are set to values based on real world. We can experience different responses if we vary the values of the bending elasticity $\xi_{\alpha\beta}$. In Figure 8.a we assigned smaller value to $\xi_{\alpha\beta}$ and the tie looks like to be silky. When we increased the value of $\xi_{\alpha\beta}$, it resembles cotton (Figure 8.b).

Figure 1 also exemplifies the importance of $\xi_{\alpha\beta}$ in cloth simulation. It contains the simulation results of a square piece under compressing forces. In four cases, we used the same combination of $\zeta_{\alpha\beta} = 400$, $\phi_{\alpha\beta} = 0.1$ and only varied the parameters $\xi_{\alpha\beta}$. We can see the sensitivity achieved for $\xi_{\alpha\beta}$. When $\xi_{\alpha\beta} = 0.01$ the square piece looks like a piece of satin cloth (Figure 1.a). For $\xi_{\alpha\beta} = 0.02$, it behaves as a piece of cotton textile (Figure 1.b). With $\xi_{\alpha\beta} = 0.04$,

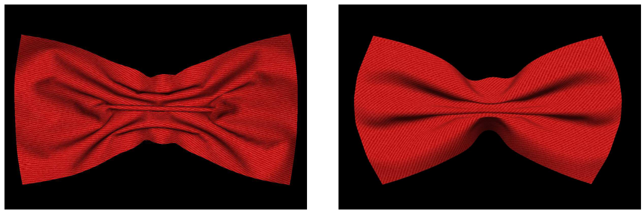

(a) (b)

Figure 8. A bow tie: (a) $\xi_{\alpha\beta} = 0.01$ and (b) $\xi_{\alpha\beta} = 0.03$.

we get something similar to jeans textile (Figure 1.c). If we increase $\xi_{\alpha\beta}$ to 0.1, we get something similar to sailcloth (Figure 1.d).

Thus, the parameter $\zeta_{\alpha\beta}$ corresponds to the surface metric resistance and as clothes in general do not change area, we can vary it in the range 100 to 400 for obtain the behavior of the most fabrics type. From 100 to 30, we get different degrees of elasticity in the composition of a cloth, and as the values get longer from this range, more than 400 and less than 30, the surface stop resembles garments. If we keep $\zeta_{\alpha\beta} = 400$ and change $\xi_{\alpha\beta}$ in the interval 0.01 to 1.0 is possible to obtain a big diversity of folds according to the surface material stiffness .

The parameter $\xi_{\alpha\beta}$ is related to the surface bending resistance and it controls the smoothness and frequency of the folds that easily appears in a clothes. The parameter $\phi_{\alpha\beta}$ couples the metric and bending strains, so the tangential forces generate perpendicular forces in a natural way, producing a more realistic visual effect. This last parameter is used in the same range of $\xi_{\alpha\beta}$, but instead that, $\phi_{\alpha\beta}$ is not so perceptible when vary values inside its range, exception in the situation that we vary from 0 to a positive and valid value (Figure 7).

Figure 9 illustrates the difference between the parameters $\xi_{\alpha\beta}$ and $\phi_{\alpha\beta}$. In the Figure 9(a) we have a flag under wind force with $\xi_{\alpha\beta} = 0.04$ and $\phi_{\alpha\beta} = 0.01$, and in Figure 9(b) we only change $\xi_{\alpha\beta}$ to 0.02. Is possible to note that in this last figure the flag have bigger frequency and smoothness of the folds. The Figures 9(c) and 9(d) show the simulations (a) and (b) with $\phi_{\alpha\beta} = 0.1$. In these last configurations, the flags clearly have more folds due to the tangential strains have more impact on the out-plane deformations, forming wrinkles, but this difference is sometimes subtle, as in draping situations (Figure. 6).

6. Conclusions

We have presented some results of an analysis of the deformable model summarized in Section 2. Our goal has been to explore the geometric potential of this model and

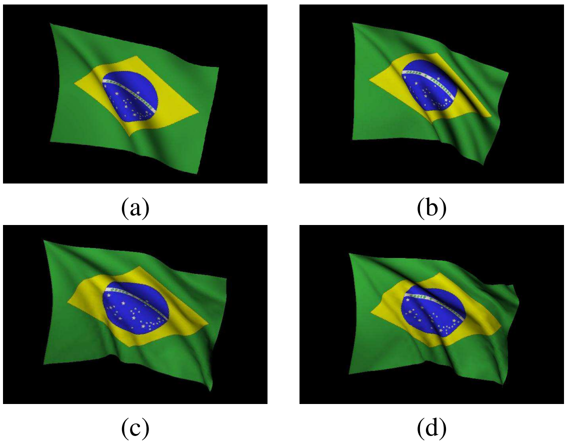

Figure 9. A flag with $\zeta_{\alpha\beta} = 400$: (a) $\xi_{\alpha\beta} = 0.04$ and $\phi_{\alpha\beta} = 0.01$, (b) $\xi_{\alpha\beta} = 0.02$ and $\phi_{\alpha\beta} = 0.01$, (c) $\xi_{\alpha\beta} = 0.04$ and $\phi_{\alpha\beta} = 1.0$, and (d)$\xi_{\alpha\beta} = 0.02$ and $\phi_{\alpha\beta} = 1.0$.

to devise a more intuitive interface for modeling cloth's responses.

We distinguished three classes of parameters that are functionally independent: material, kinematics, and simulation parameters. Since our interest was on the geometric aspect of the way that a deformable surface bends under external forces, we focused our discussion on the material parameters and develop a graphics interface (Section 3) for direct manipulate them. We showed with the procedure present in Section 4 that, although the membrane and the bending variations do not occur independently, we may represent them as independent terms and think the final effect as the superposition of effects produced by each term. Only for simulating a very typical cloth's behavior, consisting upward buckling under tangential forces, it is demanding to include the coupling term of the metric and the bending measures. Moreover, for control the frequency and smoothness in the folds formation we use a specific parameter, which is used to set the cloth bending resistance and with sensible variations inside a valid range it can reproduce several types of fabrics material.

As a further work, we would like to establish an appropriate mapping between the material parameters ($\Phi^{\alpha\beta}$ and $\Psi^{\alpha\beta}$) and the fabric properties usually given in terms of mechanical parameters, such as tensile modulus, shear modulus, bending modulus, Poisson's ratio, and the elasticity constant.

References

[1] A. Barr. Siggraph89: Course notes on topics of physically based modeling. 1989.

[2] D. E. Breen, D. H. House, and P. H. Getto. A particle-based model for simulating the draping behavior of woven cloth. *Textile Research Journal*, 64(11):663–485, November 1994.

[3] D. E. Breen, D. H. House, and M. J. Wozny. Predicting the drape of woven cloth using interacting particles. *Proceedings of the annual conference on Computer graphics and interactive techniques*, pages 365–372, July 1994.

[4] K.-J. Choi and H.-S. Ko. Stable but responsive cloth. *Proceedings of SIGGRAPH*, pages 604–611, 2002.

[5] J. Eicksen and C. Truesdell. Exact theory of stress and strain in rods and shells. *Archive for Rational Mechanics and Analysis*, pages 295–323, 1958.

[6] J. Eischen, S. Deng, and T. Clapp. Finite-element modeling and control of flexible fabric parts. *IEEE Computer Graphics and Application*, 16(5):71–80, 1996.

[7] A. E. Green, P. Naghdi, and W. Wainwright. A general theory of a cosserat surface. *Archive for Rational Mechanics and Analysis*, 20:287–308, 1965.

[8] E. Grisnpun, A. Hirani, M. Desbrun, and P. Schröder. Discrete shells. *Symposium on Computer Animation*, pages 62–67, 2003.

[9] Melo, V. F. Modelagem e controle de caimento e dobras em superfcies deformveis. Tese de doutorado, Faculdade de Engenharia Eltrica e de Computao, UNICAMP, 2004.

[10] Monteiro, L.P. and Wu, S-.T. Simulao realista de tecidos. In *SBGames 2006 Proceedings*, Recife-PE, Brasil, Setembro 2006.

[11] J. Simo and D. Fox. On a stress resultant geometrically exact shell model. part i: Formulation and optimal parameterization. *Computer Methods in Applied Mechanics and Engeneering*, (72):267–304, 1989.

[12] J. Simo and D. Fox. On a stress resultant geometrically exact shell model. part ii: The linear theory. *Computer Methods in Applied Mechanics and Engeneering*, (73):53–92, 1989.

[13] J. Simo and D. Fox. On a stress resultant geometrically exact shell model. part iii: Aspects of the nonlinear theory. *Computer Methods in Applied Mechanics and Engeneering*, (79):21–70, 1989.

[14] D. Terzopoulos, J. Platt, and A. Barr. Elastically deformable models. *Computer Graphics*, 21(4):205–214, July 1987.

[15] B. Thomaszewski, M. Wacker, and W. Straßer. A consistent bending model for cloth simulation with corotational subdivision finite elements. *Proceedings of ACM SIGGRAPH/Eurographics Symposium on Computer Animation (SCA 2006)*, pages 0–10, 2006.